Article

Cubic versus Spherical Magnetic Nanoparticles: The Role of Surface Anisotropy

G. Salazar-Alvarez, J. Qin, V. S#epela#k, I. Bergmann, M. Vasilakaki, K. N. Trohidou, J. D. Ardisson, W. A. A. Macedo, M. Mikhaylova, M. Muhammed, M. D. Baro#, and J. Nogue#s

J. Am. Chem. Soc., **2008**, 130 (40), 13234-13239 • DOI: 10.1021/ja0768744 • Publication Date (Web): 11 September 2008

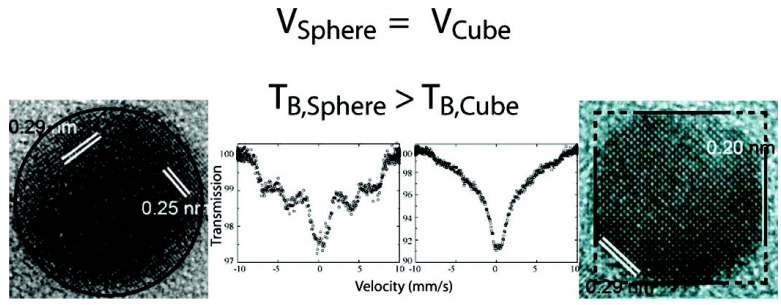

More About This Article

Additional resources and features associated with this article are available within the HTML version:

- Supporting Information
- Access to high resolution figures
- Links to articles and content related to this article
- Copyright permission to reproduce figures and/or text from this article

View the Full Text HTML

J|A|C|S
ARTICLES

Published on Web 09/11/2008

Cubic versus Spherical Magnetic Nanoparticles: The Role of Surface Anisotropy

G. Salazar-Alvarez,[†] J. Qin,[‡] V. Šepelák,[§,△] I. Bergmann,[§] M. Vasilakaki,[||] K. N. Trohidou,[||] J. D. Ardisson,[⊥] W. A. A. Macedo,[⊥] M. Mikhaylova,[#] M. Muhammed,[‡] M. D. Baró,[▽] and J. Nogués*[,○]

Institut Català de Nanotecnologia, Edifici CM7, Campus Universitat Autònoma de Barcelona, E-08193 Bellaterra (Barcelona), Spain, Materials Chemistry Division, Royal Institute of Technology, SE-100 44 Stockholm, Sweden, Institute of Physical and Theoretical Chemistry, Braunschweig University of Technology, D-38106 Braunschweig, Germany, Institute of Materials Science, NCSR Demokritos, 15310 Athens, Greece, Laboratório de Física Aplicada, Centro de Desenvolvimento da Tecnologia Nuclear, 30123-970 Belo Horizonte, Minais Gerais, Brazil, JHU ICMIC Program, Russell H. Morgan Department of Radiology and Radiological Science, School of Medicine, The Johns Hopkins University, Baltimore, Maryland 21205, Departament de Física, Universitat Autònoma de Barcelona, E-08193 Bellaterra (Barcelona), Spain, and Institució Catalana de Recerca i Estudis Avançats (ICREA) and Institut Català de Nanotecnologia, Edifici CM7, Campus Universitat Autònoma de Barcelona, E-08193 Bellaterra (Barcelona), Spain

Received September 11, 2007; E-mail: josep.nogues@uab.cat.

Abstract: The magnetic properties of maghemite (γ-Fe_2O_3) cubic and spherical nanoparticles of similar sizes have been experimentally and theoretically studied. The blocking temperature, T_B, of the nanoparticles depends on their shape, with the spherical ones exhibiting larger T_B. Other low temperature properties such as saturation magnetization, coercivity, loop shift or spin canting are rather similar. The experimental effective anisotropy and the Monte Carlo simulations indicate that the different random surface anisotropy of the two morphologies combined with the low magnetocrystalline anisotropy of γ-Fe_2O_3 is the origin of these effects.

Introduction

The interest in magnetic nanoparticles has been steadily increasing in the past decade driven both by their novel fundamental properties and the broad range of applications.[1−6] The advances in chemical synthesis methods have allowed the production of nanoparticles of different sizes with very narrow size distributions.[1−5] Moreover, most of the investigations on magnetic nanoparticles have been carried out in spherical nanoparticles, although other shapes (e.g., rods, disks, cubes, rhombohedral, tetrapods, or more complex shapes) have also been synthesized.[1−19] It should be emphasized that experimental and theoretical magnetic studies comparing nanoparticles of the same material and similar size but different shape are rather

[†] Institut Català de Nanotecnologia, Campus Universitat Autònoma de Barcelona.
[‡] Royal Institute of Technology.
[§] Braunschweig University of Technology.
[||] Institute of Materials Science.
[⊥] Centro de Desenvolvimento da Tecnologia Nuclear.
[#] The Johns Hopkins University.
[▽] Universitat Autònoma de Barcelona.
[○] Institució Catalana de Recerca i Estudis Avançats (ICREA) and Institut Català de Nanotecnologia, Campus Universitat Autònoma de Barcelona.
[△] On leave from the Slovak Academy of Sciences, Košice, Slovakia.

(1) Willard, M.; Kurihara, L. K.; Carpenter, E.; Calvin, S.; Harris, V. *Int. Mater. Rev.* **2004**, *49*, 125–170.
(2) Batlle, X.; Labarta, A. *J. Phys. D: Appl. Phys.* **2002**, *35*, R15–R42.
(3) Tartaj, P.; Morales, M.; Veintemillas-Verdager, S.; González-Carreno, T.; Serna, C. *J. Phys. D: Appl. Phys.* **2003**, *36*, R182–R197.
(4) Hyeon, T. *Chem. Commun.* **2003**, 927–934.
(5) Sun, S.; Murray, C.; Weller, D.; Folks, L.; Moser, A. *Science* **2000**, *287*, 1989–1992.
(6) Krishnan, K.; Pakhomov, A.; Bao, Y.; Blomqvist, P.; Chun, Y.; Gonzales, M.; Griffin, K.; Ji, X.; Roberts, B. K. *J. Mater. Sci.* **2006**, *41*, 793–815.
(7) Puntes, V.; Krishnan, K.; Alivisatos, A. *Science* **2001**, *291*, 2115–2117.
(8) Puntes, V.; Zanchet, D.; Erdonmez, C.; Alivisatos, A. *J. Am. Chem. Soc.* **2002**, *124*, 12874–12880.
(9) Ngo, A.; Richardi, J.; Pileni, M. *Langmuir* **2005**, *21*, 10234–10239.
(10) Margeat, O.; Tran, M.; Spasova, M.; Farle, M. *Phys. Rev. B* **2007**, *75*, 134410.
(11) Jana, N.; Chen, Y.; Peng, X. *Chem. Mater.* **2004**, *16*, 3931–3935.
(12) Bao, Y.; Beerman, M.; Krishnan, K. *J. Magn. Magn. Mater.* **2003**, *266*, L245–L249.
(13) Zitoun, D.; Pinna, N.; Frolet, N.; Belin, C. *J. Am. Chem. Soc.* **2005**, *127*, 15034–15035.
(14) Cozzoli, P.; Snoeck, E.; Garcia, M.; Giannini, C.; Guagliardi, A.; Cervellino, A.; Gozzo, F.; Hernando, A.; Achterhold, K.; Ciobanu, N.; Parak, F.; Cingolani, R.; Manna, L. *Nano Lett.* **2006**, *6*, 1966–1972.
(15) An, K.; Lee, N.; Park, J.; Kim, S.; Hwang, Y.; Park, J.; Kim, J.; Park, J.; Han, M.; Yu, J.; Hyeon, T. *J. Am. Chem. Soc.* **2006**, *128*, 9753–9760.
(16) Roca, A.; Morales, M.; O'Grady, K.; Serna, C. *Nanotechnology* **2006**, *17*, 2783–2788.
(17) Park, J.; An, K.; Hwang, Y.; Park, J.-G.; Noh, H.-J.; Kim, J.-Y.; Park, J.-H.; Hwang, N.-M.; Hyeon, T. *Nat. Mater.* **2004**, *3*, 891–895.
(18) Song, Q.; Zhang, Z. J. *J. Am. Chem. Soc.* **2004**, *126*, 6164–6168.
(19) Seo, W.; Jo, H.; Lee, K.; Kim, B.; Oh, S.; Park, J. *Angew. Chem., Intl. Ed.* **2004**, *116*, 1135–1137.

10.1021/ja0768744 CCC: $40.75

scarce.[18−23] For example, the recent investigation comparing spherical and cubic cobalt ferrite nanoparticles has shown that while the blocking temperature, T_B, and the saturation magnetization, M_S, appear to be independent of the shape, the coercivity, H_C, is larger for the spherical particles than for the cubic ones.[18] It is noteworthy that cobalt ferrite has a moderately large magnetocrystalline anisotropy $K_B(CoFe_2O_4) = 2 \times 10^6$ erg/cm^3 (ref 24).

In this article we report on the comparison of the magnetic properties of cubic and spherical nanoparticles composed of γ-Fe_2O_3 with similar sizes. We show experimentally and through Monte Carlo simulations that the difference in effective surface anisotropy between both geometries leads to substantial differences in the blocking temperature of samples with similar size due to the small intrinsic magnetocrystalline anisotropy of γ-Fe_2O_3.

Experimental Section and Modeling

The iron oleate complex was prepared following a similar procedure reported earlier:[17] 4 mmol of iron(III) chloride (Riedel-de Haën) and 12 mmol of sodium oleate (Riedel-de Haën) were dissolved in 8 mL ethanol, 6 mL deionized water, and 14 mL hexane and refluxed for 4 h. Subsequently, the organic phase was washed with deionized water three times. The cubic particles were prepared by dissolving 4 mmol of the waxy iron oleate complex and 4 mmol of oleic acid (Fluka) in 24.8 mL dioctyl ether at 70 °C. The mixture was heated to 290 °C (at 3 °C/min) and kept for 10 h. The spherical particles were prepared by dissolving 4 mmol of the iron oleate complex and 6 mmol of oleic acid in 37.2 mL dioctyl ether at 70 °C. The mixture was heated to 290 °C (at 3 °C/min) and kept for 2 h. The particle dispersions were coagulated by adding ethanol and the nanoparticles were retrieved by two cycles of centrifugation at 6000 rpm and redispersion in hexane. In the case of the sample with spherical particles, a size selection procedure was carried out in order to lower the fraction of small particles. The procedure consisted in redispersing the particles in hexane and adding a small amount of ethanol to the dispersion followed by centrifugation at 2000 rpm. The supernatant containing smaller particles was then discarded.

High-resolution transmission electron microscopy micrographs (HRTEM) were taken in a JEOL-2010 electron microscope operating at 200 kV. Magnetic measurements were carried out on loosely packed powdered samples using a superconducting quantum interference device (SQUID) magnetometer with 7.0 T maximum field. The zero-field-cooled magnetization measurements were carried out in $\mu_0 H = 2$ mT. The hysteresis loops were measured at different temperatures after field cooling in $\mu_0 H_{FC} = 1$ T. Measurements carried out on samples dispersed in paraffin resulted in virtually the same results. Zero-field Mössbauer spectra were obtained in the range 5−380 K, while in-field Mössbauer spectra were obtained at 5 K using $\mu_0 H = 5.5$ T with the field applied perpendicular to the γ-rays, both using a ^{57}Co/Rh source. Recoil spectral analysis software[25] was used for the quantitative evaluation of the Mössbauer spectra. The degree of inversion λ (the fraction of tetrahedral sites occupied by Fe^{3+} cations) was calculated from the Mössbauer subspectral intensities for the tetrahedral (A), $I_{(A)}$, and octahedral [B], $I_{[B]}$, sites according to $I_{(A)}/I_{[B]} = (f_{(A)}/f_{[B]})(\lambda/((^8/_3) - \lambda))$, assuming that the ratio of recoilless fraction is $f_{[B]}/f_{(A)} = 1$ at 5 K. The average canting angle, Ψ, was calculated from the ratio of the intensities of lines 2 and 3 from each subspectra, I_2/I_3, according to $\Psi = 90° - \arcsin(3(I_2/I_3)/2)/(1 + 3(I_2/I_3)/4)^{1/2}$.

For the Monte Carlo simulations we consider for simplicity[26] simple cubic (sc) systems with classical Heisenberg exchange interactions between the spins with the bulk and surface spins experiencing different anisotropies. Two types of particles are considered, spherical and cubic (with rounded edges). A spherical particle of radius R is defined by fixing the origin at a certain spin and including all spins within a distance of R lattice spacings, a_0. The cubic nanoparticles are formed by placing the spins at the sites of the sc lattice and to create rounded edges, we excluded the edges of the cube. To keep the volume similar to the experimental one, the size for the spherical and cubic particles were taken as 8.1 and 7 a_0, respectively.

In the presence of an external magnetic field, the total energy of the system is taken as

$$E = -\sum_i \sum_{j \neq i} J_{ij} \vec{S}_i \cdot \vec{S}_j - \sum_i K_i (S_i \cdot \hat{e}_i)^2 - \vec{H} \cdot \sum_i \vec{S}_i \qquad (1)$$

We consider nearest neighbor coupling with J_{ij} equal to $-J$ ($J > 0$). Here $\vec{S}_i$ is the atomic spin at site i and $\hat{e}_i$ is the unit vector in the direction of the easy axis at site i. The first term gives the exchange interaction between the spins in the ferrimagnetic nanoparticle (the exchange coupling constant J is taken equal to 1). The second term gives the anisotropy energy of the particle. The core anisotropy is considered uniaxial along the z-axis with anisotropy coupling constant $K_i = K_B = 0.1$ J. We take the surface thickness equal to a_0. If i lies in the outer layer of the particle then $K_i = K_S = 1.5$ J. We consider strong random axis anisotropy at the surface to model the disordered state of the surface. The third term is the Zeeman energy. Simulations fixing $K_S = 1.5$ J and varying $K_B = 0.1-3.0$ J have also been carried out. Note that H, H_C and H_E are given in units of $J/g\mu_B$, T in units J/k_B and the anisotropy constants K in units of J.

The Monte Carlo method for a Heisenberg system[27,28] was used to study the magnetic behavior of the nanoparticle. Typically, 10^4 Monte Carlo steps per spin were found to be sufficient in the simulations. The results were averaged over 10 different samples (namely, independent random number sequences that give different spin configurations) cooled down under the same conditions. Note that the statistical error is negligible. A two sublattice model is used for the ferrimagnetism, considering the size of the atomic spins in the two sublattices equal to 1 and $^3/_2$, respectively.

The zero-field cooling procedure is simulated starting from a demagnetized nanoparticle at temperature $T = 6$ J/k_B (which is above the critical temperature of the nanoparticle), cooling the nanoparticle down to $T = 0$ without a field. Subsequently, the temperature is raised to $T = 6$ J/k_B in the presence of magnetic fields along the z-axis.

Results and Discussion

As can be seen from the TEM images shown in Figure 1, the nanoparticles synthesized with a short reaction time exhibit a clear spherical character (Figure 1a) with a monodispersion of particle size ($d = 14.5$ nm with $\sigma_{\log\,\mathrm{norm}} = 0.8$ nm; and a volume, $V_{sphe} \approx 1600$ nm^3), typical for nanoparticles prepared by "dry" chemical methods.[1−5] On the other hand, the nano-

(20) Dimitrov, D. A.; Wysin, G. M. *Phys. Rev. B* **1994**, *50*, 3077–3084.
(21) Evans, R.; Nowak, U.; Dorfbauer, F.; Shrefl, T.; Mryasov, O.; Chantrell, R. W.; Grochola, G. *J. Appl. Phys.* **2006**, *99*, 08G703.
(22) Yanes, R.; Chubykalo-Fesenko, O.; Kachkachi, H.; Garanin, D. A.; Evans, R.; Chantrell, R. W. *Phys. Rev. B* **2007**, *76*, 064416.
(23) Bai, J.; Xu, Y.; Wang, J. *IEEE Trans. Magn.* **2007**, *43*, 3340–3342.
(24) Cornell, R.; Schwertmann, U. *The Iron Oxides: Structure, Properties, Reactions, Occurences and Uses*, 2nd ed.; Wiley-VCH: Weinheim, Germany, 2003.
(25) Lagarec, K.; Rancourt, D. G. *Recoil - Mössbauer Spectral Analysis Software for Windows*, v1.02; University of Ottawa: Ottawa, Canada, 1998.
(26) Trohidou, K.; Zianni, X.; Blackman, J. *IEEE Trans. Magn.* **1998**, *34*, 11201122. Note that although the choice of structure does affect the values of the extracted parameters, e.g., H_C, it does not usually affect the overall trends of the magnetic properties.
(27) Binder, K. *Applications of Monte Carlo Methods in Statistical Physics*; Springer: Berlin, 1984.
(28) Eftaxias, E.; Trohidou, K. N. *Phys. Rev. B* **2005**, *71*, 134406.

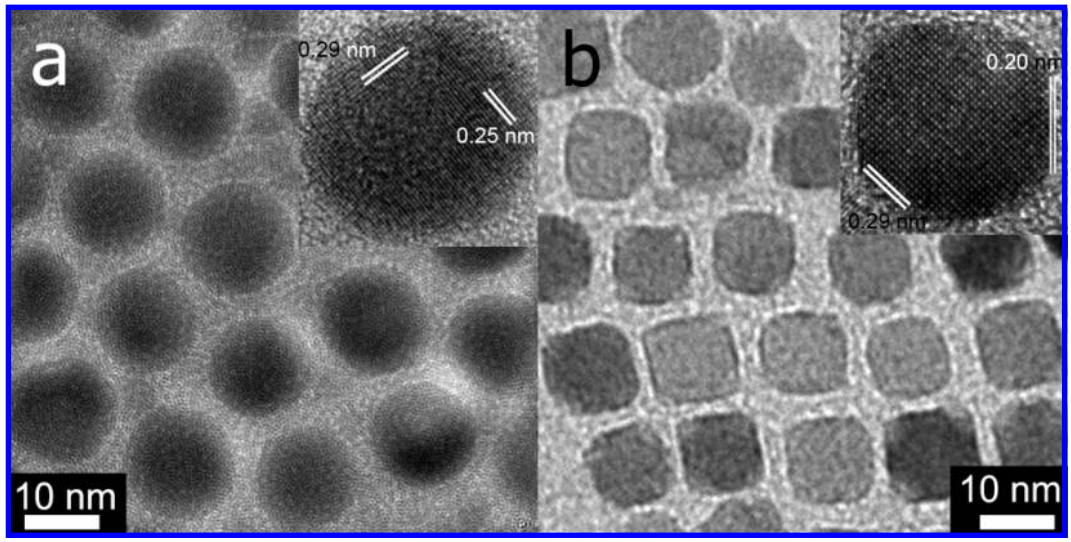

Figure 1. Transmission electron microscope (TEM) micrographs of (a) spherical and (b) cubic γ-Fe_2O_3 nanoparticles. The insets show high resolution (HRTEM) images of the respective nanoparticles. The lattice fringes are indicated in the insets. Note that the lattice fringes corresponding to the (400) reflections (0.20 nm) are parallel to the cube edges.

particles synthesized with a long reaction time exhibit a cubic shape with rounded edges (Figure 1b) with an edge length of $l = 12$ nm and a narrow size distribution $\sigma_{\log\,\mathrm{norm}} = 2.5$ nm (hereon we will use d to denote both diameter and edge length). The high resolution images show that the cubic particles consist of low-energy {100} faces, in agreement with previous reports.[18,29] The lattice fringes of both types of particles are indexed to those of cubic spinel structure (JCPDS Card no. 391346). The average volume of the cubic nanoparticles, $V_{\mathrm{cub}} \approx 1700$ nm^3, is similar to that of the spherical ones with $V_{\mathrm{sphe}} \approx 1600$ nm^3. Interestingly, the prolonged time needed to obtain cubic nanoparticles allows for the Ostwald ripening of the small particles, which are then dissolved and incorporated into the larger ones contributing to a broader size distribution.[30−32] In the case of the sample containing the spherical particles some small particles (with a size of about 3 nm) generated during the synthesis, about 10 vol %, could be lowered by size selection procedures to about 5 vol % and do not contribute to a particle size broadening. The crystallographic composition was further assessed by X-ray powder diffraction (see Supporting Information, Figure S1). Rietveld analysis of the diffraction data shows that both types of particles consisted of a spinel structure with a lattice parameter $a_0 = 0.836$ nm and a ratio of octahedral, [B], to tetrahedral, (A), sites of ca. [B]/(A) = 2 consistent with that of disordered cubic spinel structure.[24] Similar synthesis methods are reported to yield magnetite,[17] nevertheless, it is known that magnetite oxidizes topotactically to maghemite upon exposure to air.[24] Hence, it is safe to assume that the final product has a composition near that of disordered maghemite. Hence, although the samples have different morphology, their crystal structure is similar.

Despite their structural similarity, magnetically the two types of nanoparticles exhibit some distinct differences. As can be seen from the room-temperature zero-field Mössbauer spectroscopy spectra, the spherical nanoparticles appear as more magnetically ordered (i.e., with the presence of a better resolved magnetically split component superposed to the superparamagnetic doublet) than the cubic ones even having a similar volume (see Figure 2).[33] However, zero-field Mössbauer spectroscopy at low temperatures, where both types of nanoparticles are magnetically blocked, shows that the basic parameters such as magnetic hyperfine fields, quadrupole splitting, and isomer shift of both samples are identical within the experimental error, indicating similar microscopic magnetic structure, in agreement with their similar crystalline structure (see Supporting Information for details).

The zero-field-cooled (ZFC) magnetization measurements show that the average blocking temperature, $T_{\mathrm{B}}^{M(T)}$, obtained from the maximum at M^{ZFC}, as shown in Figure 3, of the spherical nanoparticles ($T_{\mathrm{B}}^{M(T)}$(sphe) $\approx 235 \pm 2$ K) is larger than the cubic ones ($T_{\mathrm{B}}^{M(T)}$(cub) $\approx 190 \pm 2$ K) in agreement with the room temperature Mössbauer spectra.[34−36] A similar result is obtained when analyzing the temperature dependence of the coercivity (see Supporting Information Figure S2). For instance, it is found that fitting the $H_{\mathrm{C}}(T)$ curves with the typical Stoner−Wohlfart model,[37] that is, $H_{\mathrm{C}}(T) = H_{\mathrm{C}}(0)(1 - T/T_{\mathrm{B}}^{H_{\mathrm{C}}})^{1/2}$, where $T_{\mathrm{B}}^{H_{\mathrm{C}}}$ is the temperature at which the magnetization curves show no coercivity or remanence, we find for spherical and cubic particles that $T_{\mathrm{B}}^{H_{\mathrm{C}}}$(sphe) $= 112 \pm 10$ K and $T_{\mathrm{B}}^{H_{\mathrm{C}}}$(cub) $= 87 \pm 10$ K, respectively. T_{B} was also assessed from the temperature dependence of the Mössbauer spectra as the temperature at

(29) Davies, M. J.; Parker, S. C.; Watson, G. W. *J. Mater. Chem.* **1994**, *4*, 813–816.
(30) Lifshitz, I. M.; Slyozov, V. V. *J. Phys. Chem. Solid* **1961**, *19*, 35–50.
(31) Wagner, C. *Elektrochemie* **1961**, *65*, 581–591.
(32) Ozkam, G. *J. Sol-Gel Sci. Technol.* **2006**, *37*, 161–164.
(33) Note that given the different measuring times from Mössbauer and magnetization measurements, the exact T_{B} obtained from each measurement should be different since $T_{\mathrm{B}} = K_{\mathrm{eff}}V/(k_{\mathrm{B}} \ln(\tau_{\mathrm{m}}/\tau_0))$, where τ_0 is the inverse of the attempt frequency and τ_{m} is a time characteristic for each measuring technique.
(34) Note that due to the concomitant dipolar interactions the ZFC curve becomes broader and the determination of T_{B} from $M(T)$ becomes less reliable. However, since the measuring conditions are the same for both samples, the ratio T_{B}(sphe)/T_{B}(cub) should be more consistent.
(35) Vargas, J.; Socolovsky, L.; Knobel, M.; Zanchet, D. *Nanotechnology* **2005**, *16*, S285–S290.
(36) Allia, P.; Coisson, M.; Tiberto, P.; Vinai, F.; Knobel, M.; Novak, M. A.; Nunes, W. C. *Phys. Rev. B* **2001**, *64*, 144420.
(37) Martinez, B.; Roig, A.; Obradors, X.; Molins, E.; Rouanet, A.; Monty, C. *J. Appl. Phys.* **1996**, *79*, 2580–2586.
(38) Rebbouh, L.; Hermann, R. P.; Grandjean, F.; Hyeon, T.; An, K.; Amato, A.; Long, G. J. *Phys. Rev. B* **2007**, *76*, 174422.

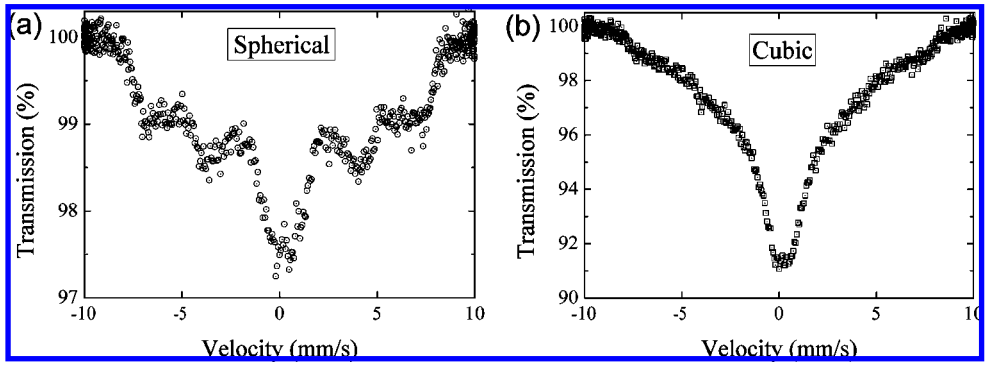

Figure 2. Zero field Mössbauer spectra at room temperature for (a) spherical and (b) cubic γ-Fe_2O_3 nanoparticles.

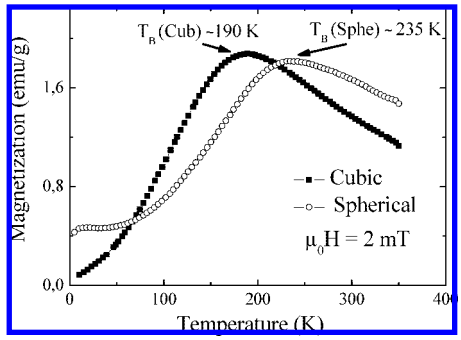

Figure 3. Temperature dependence of the zero field cooled magnetization for the spherical (○) and cubic (■) γ-Fe_2O_3 nanoparticles. The blocking temperature of the spherical [T_B(sphe)] and cubic [T_B(cub)] nanoparticles are indicated by arrows.

which the area of the split spectrum and the superparamagnetic spectrum are equivalent, T_B^{Moss} (see Supporting Information, Figure S3). The results, $T_B^{Moss}(sphe) = 380 \pm 20$ K $> T_B^{Moss}(cub) = 350 \pm 20$ K, are consistent with the $M(T)$ and $H_C(T)$ analyses and also with recent Mössbauer results for monodispersed maghemite nanoparticles of similar size.[38] Although, as expected, the T_B obtained form the different approaches are different, the difference in T_B between the cubic and spherical nanoparticles, ΔT_B, is similar for the three techniques, $\Delta T_B^{M(T)} = 45 \pm 3$ K, $\Delta T_B^{H_C} = 25 \pm 15$ K, $\Delta T_B^{Moss} = 30 \pm 20$ K.

Interestingly, the low temperature coercivity after field cooling of the cubic samples ($\mu_o H_C(cub) = 33$ mT) is slightly larger than for the spherical ones ($\mu_o H_C(sphe) = 30$ mT). Further, a small loop shift along the field axis ($\mu_o H_E \approx 5$ mT) is observed in both samples after field cooling (see Supporting Information, Figure S4). Conversely, the low temperature magnetization studies show that the saturation magnetization of both nanoparticles is the same, $M_S = 75 \pm 1$ emu/g of Fe_2O_3 for both samples. These values are rather close to what is expected for bulk maghemite.[39,40]

To elucidate this apparent contradiction of the results, in-field Mössbauer spectroscopy was carried out. As can be seen in Figure 4, the low temperature spectra at high fields for both samples show an intensity ratio between lines 2 and 3 at high fields of $I_2/I_3 \approx 3.3$. Note that $I_2/I_3 = 4.0$ is expected if the spins align with the field for fields applied perpendicular to the γ-rays. This indicates the presence of surface spin canting, which from the ratio of the intensities of the lines 2 and 3, can be inferred to be about 17.5° for both samples. Actually, large average canting is usually correlated with increased surface anisotropy[39,41] although no univocal correlation has been established since different effects can affect spin canting in nanoparticles.[42−44]

According to Néel's pair anisotropy model, the surface anisotropy depends on the direction of the local magnetization as measured from the bond direction.[45] The origin of the surface anisotropy is mainly due to local symmetry breaking which could originate from many different effects at the surface, such as the presence of structural defects (e.g., facets), broken exchange bonds, different number of neighbors, different atomic distances (surface strain) and so on. Some of these parameters can clearly differ in cubic or spherical shapes, especially in nanoparticles. For example, the surface of a spherical nanoparticle at this size can be considered as formed from different nanofacets,[46] while the cubic nanoparticles have fairly flat faces. Thus, although spin canting is similar in both samples, the different morphology of the nanoparticles results in a larger "surface disorder" and consequently an enhanced "effective" surface anisotropy in the spherical nanoparticles. In fact, due to symmetry reasons the first order surface anisotropy effects should cancel out in both structures. Consequently, any structural defect breaking the symmetry should enhance the overall surface anisotropy. In a sense, the difference in surface anisotropy between the spherical and cubic nanoparticles is analogous to the increase in surface anisotropy in thin films with increased faceted surfaces or large curvature[47,48] or the need to artificially introduce "roughness" in the simulations of oxide nanoparticles to obtain better quantitative agreement between theoretical and experimental results.[49] In fact, γ-Fe_2O_3 nanoparticles are known to have relatively large surface anisotropies ($K_S(\gamma\text{-}Fe_2O_3) = 2-9 \times 10^{-2}$ erg/cm^2)[50−53] which lead to effective anisotropies,

(39) Coey, J. M. D. *Phys. Rev. Lett.* **1971**, *27*, 1140–1142.
(40) Dutta, P.; Manivannan, A.; Seehra, M. S.; Shah, N.; Huffman, G. P. *Phys. Rev. B* **2004**, *70*, 174428.
(41) Tronc, E.; Ezzir, A.; Cherkaoui, R.; Chanéac, C.; Nogues, M.; Kachkachi, H.; Fiorani, D.; Testa, A. M.; Greneche, J. M.; Jolivet, J. P. *J. Magn. Magn. Mater.* **2000**, *221*, 63–79.
(42) Morrish, A. H.; Haneda, K. *J. Magn. Magn. Mater.* **1983**, *35*, 105–113.
(43) Tronc, E.; Prené, P.; Jolivet, J. P.; Dormann, J. L.; Greneche, J. M. *Hyperfine Interact.* **1998**, *112*, 97–100.
(44) Hendriksen, P. V.; Linderoth, S.; Oxborrow, C. A.; Mørup, S. *J. Phys.: Condens. Matter* **1994**, *6*, 3091–3100.
(45) Néel, L. *J. Phys. Rad.* **1954**, *15*, 225–239.
(46) Jamet, M.; Wernsdorfer, W.; Thirion, C.; Dupuis, V.; Mélinon, P.; Pérez, A.; Mailly, D. *Phys. Rev. B* **2004**, *69*, 024401.
(47) Rickart, M.; Mewes, T.; Demokritov, S. O.; Hillebrands, B.; Scheib, M. *Phys. Rev. B* **2004**, *70*, 060408.
(48) Cheng, R.; Bader, S. D.; Fradin, F. Y. *Phys. Rev. B* **2008**, *77*, 024404.
(49) Kodama, R. H.; Berkowitz, A. E. *Phys. Rev. B* **1999**, *59*, 6321–6336.

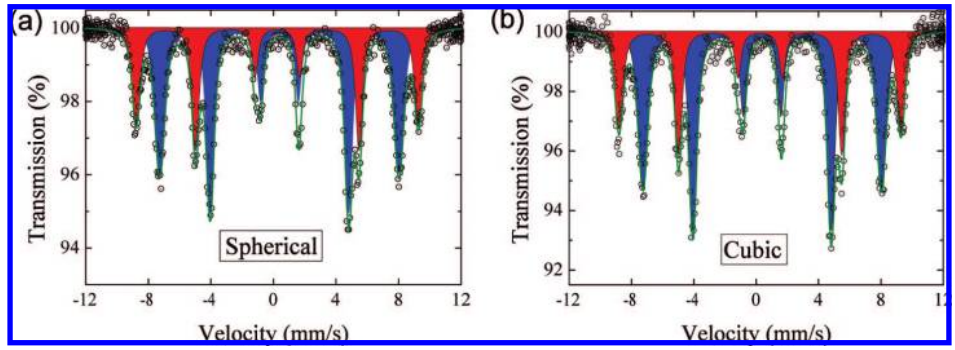

Figure 4. Mössbauer spectra of (a) spherical and (b) cubic γ-Fe_2O_3 nanoparticles. Spectra were taken at 5 K in the presence of an external magnetic field of 5.5 T applied perpendicular to the γ-ray direction. The subspectra corresponding to tetrahedrally and octahedrally coordinated Fe^{3+} cations are denoted by red and blue color, respectively.

K_{eff} (defined as $K_{eff} = K_B + 6K_S/d$)[54] in nanoparticles much larger than the bulk magnetocrystalline anisotropy ($K_B(\gamma\text{-}Fe_2O_3) = 4.7 \times 10^4$ erg/cm^3).[24] Hence, for nanoparticles with small bulk anisotropy the contribution of the surface anisotropy can be dominant. Thus, taking into account that T_B is defined as $T_B = K_{eff}V/25k_BT$, the difference in T_B between both samples implies that K_{eff}(sphe) > K_{eff}(cub) and consequently K_S(sphe) > K_S(cub), as we would expect from a larger surface disorder of the former. Comparing the T_B of both types of nanoparticles, it can be inferred that K_S(sphe) $\approx 1.5K_S$(cub).

The difference in effective anisotropies for both samples has been confirmed by Mössbauer spectroscopy, through the temperature dependence of the magnetic hyperfine field (B_{HF}). At low temperatures both samples exhibit a linear behavior of $B_{HF}(T)$ (see Supporting Information Figure S5), however the slope of the curve for the spherical one is smaller. From the empirical relation $B_{HF}(T) = B_o[1 - k_BT/2K_{eff}V]$ (ref 55) and given the volume of each particle, the relation K_{eff}(sphe)/K_{eff}(cub) = 1.08 can be inferred, consistent with the results from T_B.

Moreover, in-field Mössbauer spectroscopy has also detected a slight inversion of the vacancies. While the spherical particles exhibit perfect inverse spinel structure $(Fe_1)[Fe_{1.67}\square_{0.33}]O_4$, the cubic ones have some vacancies in the tetrahedral positions, that is, $(Fe_{0.97}\triangle_{0.03})[Fe_{1.70}\square_{0.30}]O_4$ (where $\triangle$ denotes tetrahedral vacancies). Actually, it is known that in γ-Fe_2O_3 the ordering of the vacancies can influence the magnetic properties. However, any increase in anisotropy is usually accompanied by marked decrease of M_S, or increase of the irreversibility field and the high field susceptibility.[56−58] The fact that in our case all parameters except the anisotropy remain virtually unchanged indicates that vacancy disorder does not play any critical role in the observed effects.

Finally, concerning field cooled coercivities and loop shifts, these are well know effects of core−shell exchange interaction (exchange bias)[59] and have been reported in γ-Fe_2O_3 nanoparticles assuming a ferrimagnetic core and spin-glass shell.[60,61] However, since this is a surface effect, it depends on the inverse of the linear dimensions (i.e., diameter or edge lengths), rather than the volume, as would be the case for T_B. Thus, to compare values for different samples, the interface coupling energy, $E_A = H_E \cdot M_S \cdot d/6$ is usually used.[59] Since the diameter of the spherical nanoparticle is larger than the edge of the cubic one the interface coupling energy for the spherical nanoparticle is larger than for the cubic one, E_A(sphe) $= 4.0 \times 10^{-3}$ erg/cm^2 > E_A(cub) $= 3.3 \times 10^{-3}$ erg/cm^2, consistent with the larger surface anisotropy of the former. However, H_C is more complex, since although it is known that it is also affected by the exchange coupling in the core−shell structure,[59] the change in shape can also lead to other effects, such as different reversal modes, which could influence it.[62]

When comparing the present results to the ones in cobalt ferrite,[18] it should be pointed out that $CoFe_2O_4$ is known to also have disordered surface spins.[63,64] However, because of the rather large K_B, the effects of the surface anisotropy become evident only at very small sizes ($d < 5$ nm).[64] In the study by Song and Zhang, while spherical nanoparticles with $d < 5$ nm were studied, all the cubic ones were larger than $d = 8$ nm.[18] Thus, the surface anisotropy effects discussed in this article were less evident in their study.

Monte Carlo simulations, performed in spheres and cubes (with rounded edges) with sizes analogous to the experimental ones, agree qualitatively with the experimental results. As shown in Figure 5a the spherical nanoparticles exhibit a higher T_B (i.e., proportional to the maximum in m_z^{ZFC}) than the cubic ones. As can be seen in the inset, the difference between T_B of the

(50) Gazeau, F.; Bacri, J. C.; Gendron, F.; Perzynski, R.; Raikher, Y. L.; Stepanov, V. I.; Dubois, E. *J. Magn. Magn. Mater.* **1998**, *186*, 175–187.
(51) Dormann, J. L.; d'Orazio, F.; Lucari, F.; Tronc, E.; Prene, P.; Jolivet, J. P.; Fiorani, D.; Cherkaoui, R.; Nogues, M. *Phys. Rev. B* **1996**, *53*, 14291–14297.
(52) Tronc, E.; Prene, P.; Jolivet, J. P.; d'Orazio, F.; Lucari, F.; Fiorani, D.; Godinho, M.; Cherkaoui, R.; Nogues, M.; Dormann, J. L. *Hyperfine Interact.* **1995**, *95*, 129–148.
(53) Tartaj, P.; Serna, C. J. *Chem. Mater.* **2002**, *14*, 4396–4402.
(54) Bødker, F.; Mørup, S.; Linderoth, S. *Phys. Rev. Lett.* **1994**, *72*, 282–285.
(55) Mørup, S. *J. Magn. Magn. Mater.* **1983**, *37*, 39–50.
(56) Morales, M. P.; Serna, C. J.; Bødker, F.; Mørup, S. *J. Phys.: Condens. Matter* **1997**, *9*, 5461–5467.
(57) Morales, M. P.; Veintemillas-Verdaguer, S.; Montero, M. I.; Serna, C. J.; Roig, A.; Casas, L.; Martnez, B.; Sandiumenge, F. *Chem. Mater.* **1999**, *11*, 3058–3064.
(58) Feltin, N.; Pileni, M. P. *Langmuir* **1997**, *13*, 3927–3933.
(59) Nogués, J.; Sort, J.; Langlais, V.; Skumryev, V.; Surinach, S.; Munoz, J. S.; Baró, M. D. *Phys. Rep.* **2005**, *422*, 65–117.
(60) Martnez, B.; Obradors, X.; Balcells, L.; Rouanet, A.; Monty, C. *Phys. Rev. Lett.* **1998**, *80*, 181–184.
(61) Cannas, C.; Concas, G.; Gatteschi, D.; Falqui, A.; Musinu, A.; Piccaluga, G.; Sangregorio, C.; Spano, G. *Phys. Chem. Chem. Phys.* **2001**, *3*, 832–838.
(62) Skomski, R. *J. Phys.: Condens. Matter* **2003**, *15*, R841–R896.
(63) Haneda, K.; Morrish, A. H. *J. Appl. Phys.* **1988**, *63*, 4258–4260.
(64) Ngo, A. T.; Bonville, P.; Pileni, M. P. *J. Appl. Phys.* **2001**, *89*, 3370–3376.

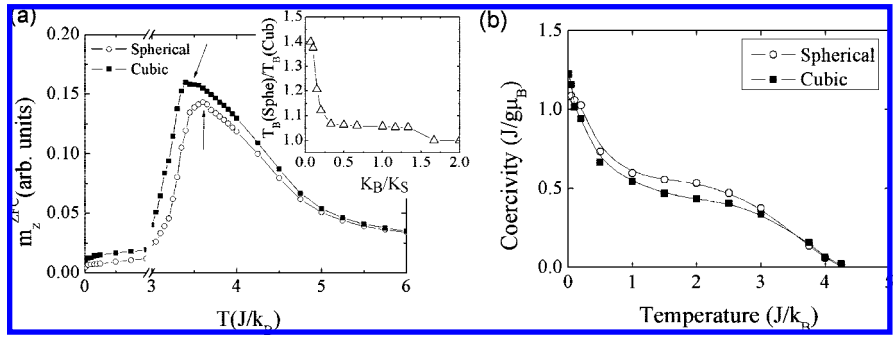

Figure 5. (a) Temperature dependence of the zero-field-cooled magnetization along the easy axis, m_z^{ZFC}, for the cubic and spherical nanoparticles obtained from the simulations with $K_S = 1.5$ J and $K_B = 0.1$ J with a measuring field of $H = 0.2$ J/$g\mu_B$. The blocking temperature of the spherical [T_B(sphe)] and cubic [T_B(cub)] nanoparticles are indicated by arrows. Shown in the inset is the ratio of T_B values for the spherical and cubic nanoparticles, T_B(sphe)/T_B(cub), as a function of the ratio of bulk anisotropy (K_B) to surface anisotropy (K_S), K_B/K_S, maintaining $K_S = 1.5$ J constant. (b) Temperature dependence of the coercivity, H_C, for spherical (○) and cubic (■) nanoparticles obtained from the Monte Carlo simulations for $K_S = 1.5$ J and $K_B = 0.1$ J with a cooling field of $H = 0.7$ J/$g\mu_B$. Note that the error bars are smaller than the symbols and the lines are guides to the eye.

spherical and cubic samples becomes progressively smaller as the bulk anisotropy used in the simulation becomes larger (maintaining the surface anisotropy constant). This is consistent with the comparison of the present results (i.e., small K_B) and the ones for cobalt ferrite in ref 18 (i.e., large K_B). As regards to the coercivity, the simulations reproduce nicely the cross over in $H_C(T)$ observed experimentally (see Figure 5b). Namely, while at low temperatures H_C(cub) > H_C(sphe), as the temperature increases the spherical particles have larger H_C. However, in contrast to experiments, the temperature at which H_C becomes zero is similar for both types of nanoparticles. Nevertheless, this can be considered as a moderate agreement, since for the nominal sizes (volumes) used in the simulations one should expect ($T(H_C = 0)$) to be larger for the cubic samples. Finally, note that similar to the experimental results the simulations also exhibit loop shifts, where H_E is typically 10 times smaller than H_C in accordance to what is observed experimentally. Analysis of the simulations evidence that owing to the morphology of the particles, the spherical ones tend to have more uncompensated spins at the surface. Moreover, owing to the presence of the imposed random surface anisotropy the spins at the surface show some canting (in agreement with the in-field Mössbauer measurements). The presence of uncompensated spins and canting strongly influences the magnetic response of the nanoparticles. For example, the nanoparticles exhibit an incoherent reversal, with clusters of spins switching independently, rather than the coherent reversal expected for these sizes (see Supporting Information Figure S6). This kind of switching is dominated by the details (e.g., canting) of the surface spins.

Conclusions

We have shown that the blocking temperature of γ-Fe_2O_3 nanoparticles is larger for spherical nanoparticles than for cubic ones, despite having similar volumes. From the experimental data and the Monte Carlo simulations this behavior is ascribed to the role played by the morphology of the nanoparticles on the effective surface anisotropy of the samples and the small intrinsic anisotropy of γ-Fe_2O_3.

Acknowledgment. This work was supported by the Spanish CICYT (MAT2007-66302-C02), MEC (CSD2006-00012 Consolider-Ingenio 2010), the Catalan DGR (2005-SGR-00401), and the Institut Català de Nanotecnologia. The authors thank the Serveis de Microscòpia and d'Anàlisi Química at UAB for their technical assistance. V.Š. and I.B. thank the Deutsche Forschungsgemeinschaft, APVV (Project 0728-07) and VEGA (Grant 2/0065/08) for the support of their work. WAAM acknowledges the support from the Brazilian MCT/CNPq (Proc. 475392/2006-0 and Instituto do Milênio de Nanotecnologia).

Supporting Information Available: Additional figures regarding the structural and magnetic characterization. This material is available free of charge via the Internet at http://pubs.acs.org.

JA0768744